2-2015

Formation of the oxygen torus in the inner magnetosphere: Van Allen Probes observations

M. Nose
Kyoto University

S. Oimatsu
Kyoto University

K. Keika
Nagoya University

C. A. Kletzing
University of Iowa

W. S. Kurth
University of Iowa

See next page for additional authors

Recommended Citation

M. Nosé, S. Oimatsu, K. Keika, C. A. Kletzing, W. S. Kurth, S. D. Pascuale, C. W. Smith, R. J. MacDowall, S. Nakano, G. D. Reeves, H. E. Spence, and B. A. Larsen, 'Formation of the oxygen torus in the inner magnetosphere: Van Allen Probes observations', Journal of Geophysical Research: Space Physics, vol. 120, no. 2, pp. 1182–1196, Feb. 2015.

AGU PUBLICATIONS

JGR

Journal of Geophysical Research: Space Physics

RESEARCH ARTICLE

10.1002/2014JA020593

Key Points:
- An oxygen torus is identified at L = 3.0–4.5 during the storm recovery phase
- The oxygen torus extends around the plasmapause
- The formation process of the oxygen torus is examined with numerical simulation

Correspondence to:
M. Nosé,
nose@kugi.kyoto-u.ac.jp

Citation:
Nosé, M., et al. (2015), Formation of the oxygen torus in the inner magnetosphere: Van Allen Probes observations, *J. Geophys. Res. Space Physics*, *120*, 1182–1196, doi:10.1002/2014JA020593.

Received 10 SEP 2014
Accepted 17 JAN 2015
Accepted article online 24 JAN 2015
Published online 19 FEB 2015
Corrected 6 MAR 2015

This article was corrected on 6 MAR 2015. See the end of the full text for details.

Formation of the oxygen torus in the inner magnetosphere: Van Allen Probes observations

M. Nosé[1], S. Oimatsu[2], K. Keika[3], C. A. Kletzing[4], W. S. Kurth[4], S. De Pascuale[4], C. W. Smith[5], R. J. MacDowall[6], S. Nakano[7], G. D. Reeves[8], H. E. Spence[5], and B. A. Larsen[8]

[1]Data Analysis Center for Geomagnetism and Space Magnetism, Graduate School of Science, Kyoto University, Kyoto, Japan, [2]Department of Geophysics, Graduate School of Science, Kyoto University, Kyoto, Japan, [3]Solar-Terrestrial Environment Laboratory, Nagoya University, Nagoya, Japan, [4]Department of Physics and Astronomy, University of Iowa, Iowa City, Iowa, USA, [5]Institute for Earth, Oceans and Space, University of New Hampshire, Durham, New Hampshire, USA, [6]Solar System Exploration Division, Goddard Space Flight Center, Greenbelt, Maryland, USA, [7]Institute of Statistical Mathematics, Research Organization of Information and Systems, Tokyo, Japan, [8]Space Sciences and Applications Group, Los Alamos National Laboratory, Los Alamos, New Mexico, USA

Abstract We study the formation process of an oxygen torus during the 12–15 November 2012 magnetic storm, using the magnetic field and plasma wave data obtained by Van Allen Probes. We estimate the local plasma mass density (ρ_L) and the local electron number density (n_{eL}) from the resonant frequencies of standing Alfvén waves and the upper hybrid resonance band. The average ion mass (M) can be calculated by $M \sim \rho_L / n_{eL}$ under the assumption of quasi-neutrality of plasma. During the storm recovery phase, both Probe A and Probe B observe the oxygen torus at L = 3.0–4.0 and L = 3.7–4.5, respectively, on the morning side. The oxygen torus has M = 4.5–8 amu and extends around the plasmapause that is identified at $L \sim$3.2–3.9. We find that during the initial phase, M is 4–7 amu throughout the plasma trough and remains at ~1 amu in the plasmasphere, implying that ionospheric O^+ ions are supplied into the inner magnetosphere already in the initial phase of the magnetic storm. Numerical calculation under a decrease of the convection electric field reveals that some of thermal O^+ ions distributed throughout the plasma trough are trapped within the expanded plasmasphere, whereas some of them drift around the plasmapause on the dawnside. This creates the oxygen torus spreading near the plasmapause, which is consistent with the Van Allen Probes observations. We conclude that the oxygen torus identified in this study favors the formation scenario of supplying O^+ in the inner magnetosphere during the initial phase and subsequent drift during the recovery phase.

1. Introduction

An oxygen torus is found in the deep inner magnetosphere as an enhancement of O^+ ion density in a limited range of L shell. It was first reported by *Chappell* [1982] who used the retarding ion mass spectrometer (RIMS) instrument carried by the Dynamic Explorer (DE) 1 satellite. The DE 1/RIMS instrument can measure thermal (0–45 eV) ion fluxes with mass and charge information [*Chappell et al.*, 1981] and has been used by subsequent studies to investigate characteristics of the oxygen torus. *Horwitz et al.* [1984, 1986] showed that the O^+ density sometimes becomes comparable to or exceeds the H^+ density at L = 3–4. *Roberts et al.* [1987] revealed that the heavy ion density enhancement is observed generally close to the plasmapause at all local times with higher occurrence frequency in the late evening and morning sectors. *Comfort et al.* [1988] reported that the O^+/H^+ density ratio has a peak at L = 3–5 and is larger on the evening side than on the morning side. Although the operation of the RIMS instrument was terminated in 1989, *Fraser et al.* [2005] analyzed its archived data and reported the oxygen torus. Here is a caveat: "torus" is a term originally given by *Chappell* [1982] and *Horwitz et al.* [1984] to indicate the possibility of azimuthal revolution of the O^+ density enhancement. There have, however, been no clear observational evidences of a well-defined pattern in azimuth.

After the termination of the DE 1/RIMS operation, no plasma instruments have been able to directly measure thermal O^+ ion flux to identify the oxygen torus. Instead, an indirect method for detecting the oxygen torus has been proposed. In this method, the resonant frequency of standing Alfvén waves (f) and the upper hybrid resonance band (f_{UHR}) observed by satellites are used to estimate the plasma mass density

(ρ) and the electron number density (n_e), respectively. *Singer et al.* [1981] derived the MHD wave equation in an arbitrary magnetic field geometry in the following form:

$$\frac{\partial^2}{\partial s^2}\left(\frac{\xi(s)}{h(s)}\right)+\frac{\partial}{\partial s}\ln\left\{h(s)^2B(s)\right\}\frac{\partial}{\partial s}\left(\frac{\xi(s)}{h(s)}\right)+\left(2\pi f\frac{\sqrt{\mu_0\rho(s)}}{B(s)}\right)^2\left(\frac{\xi(s)}{h(s)}\right)=0, \tag{1}$$

where s represents the distance along the magnetic field line; ξ is the displacement of the magnetic field line; h is a factor describing separation between two adjacent file lines, which becomes smaller with distance from the equator; μ_0 is the vacuum permeability; and B is the magnitude of the magnetic field. The distribution of ρ along the field line is usually modeled by a power law:

$$\rho(s)=\rho_{\mathrm{eq}}\left(\frac{r_{\mathrm{eq}}}{r}\right)^{\alpha}, \tag{2}$$

where ρ_{eq} is the equatorial plasma mass density, r is the geocentric distance to the field line at s, r_{eq} is the geocentric distance to the field line at the equator, and α is the power law index. Then the MHD equation can be solved numerically to derive ρ_{eq} which sets the standing wave between the northern and southern ionospheres. The upper hybrid resonance frequency can be written as

$$f_{\mathrm{UHR}}=\frac{1}{2\pi}\sqrt{\frac{n_e e^2}{\epsilon_0 m_e}+\left(\frac{eB}{m_e}\right)^2}, \tag{3}$$

where e is the electron charge, ϵ_0 is the vacuum permittivity, and m_e is the electron mass. Using this equation, we can estimate n_e from f_{UHR}. Once ρ and n_e are obtained, the average ion mass (M) can be calculated by $M=(\rho-n_e m_e)/n_i\sim\rho/n_i\sim\rho/n_e$ under the assumption of quasi-neutrality of plasma, where n_i is the ion number density. In 100% H^+ plasma, we have $M=1$ amu, whereas in 50% H^+ and 50% O^+ plasma, M is increased to 8.5 amu. Thus, we can infer the concentration of heavy ions from M and detect the oxygen torus.

Takahashi et al. [2006] applied this indirect method to the magnetic field and plasma wave data obtained by the Combined Release and Radiation Effects Satellite (CRRES) and found that M in the plasma trough has a median value of 3.0 amu and depends on geomagnetic activity. *Takahashi et al.* [2008] also used the CRRES data and reported an oxygen torus with $M=6$–8 amu in the plasma trough ($L=4$–5.5) interposed between the plasmasphere and the plasma plume. *Nosé et al.* [2011] examined four events of the CRRES observations and found the oxygen torus with $M>7$ amu at $L=4.5$–6.5 in the vicinity of the plasmapause. *Takahashi et al.* [2014] derived ρ_{eq} from the Geotail satellite data by solving equations (1) and (2) and demonstrated that the $F_{10.7}$ dependence of ρ_{eq} is stronger at $L\sim7$ than at $L=11$. They proposed the oxygen torus around the geosynchronous orbit as one of factors which contribute to the strong $F_{10.7}$ dependence at lower L.

In both studies by *Takahashi et al.* [2008] and *Nosé et al.* [2011], the oxygen torus was observed during the recovery phase of magnetic storms. The preference of the oxygen torus for the recovery phase has been also noted by the DE 1/RIMS observations. *Horwitz et al.* [1984] found the oxygen torus during a sharp decrease in geomagnetic activity. *Roberts et al.* [1987] showed that the occurrence frequency of the oxygen torus was still fairly high during a low *Kp* case (*Kp* = 0–2+). We suppose that this feature is related to a formation mechanism of the oxygen torus. In this study, therefore, we focus on the evolution process of an oxygen torus during a magnetic storm that occurred in November 2012 by analyzing the magnetic field and plasma wave data from the Van Allen Probes.

This paper is organized as follows. Section 2 describes the instrumentation and data set used in this study. In section 3, we demonstrate measurements of the Van Allen Probes during the recovery phase of a magnetic storm that occurred on 15 November 2012, in which an oxygen torus is identified. Section 4 repeats similar analysis for data before 15 November 2012 and examines the formation process of the oxygen torus. In section 5 we discuss the possible mechanisms of oxygen torus formation and perform numerical calculation of thermal O^+ ion drift under a decrease of the convection electric field. Results of the numerical calculation are compared with the Van Allen Probes observations. We also compare the oxygen torus with the warm plasma cloak, which was reported by previous studies, in terms of their morphology. Measurements of suprathermal ion fluxes during the appearance of the oxygen torus are then examined. Section 6 provides the conclusions of this study.

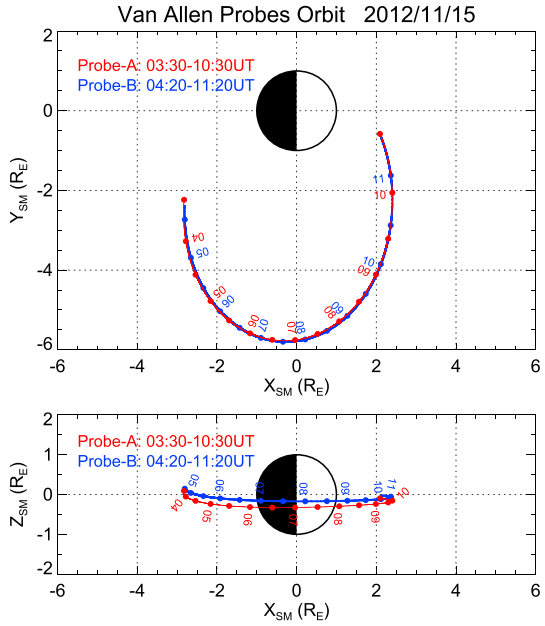

Figure 1. Orbit of Probe A (red) during 0330–1030 UT on 15 November 2012 and orbit of Probe B (blue) during 0420–1120 UT on the same day in solar magnetic (SM) coordinates. Small dots on the orbits indicate locations of probes at integer and half past hours.

2. Instrumentation and Data Set

2.1. Van Allen Probes

The Van Allen Probes consists of two identical spacecraft and were launched on 30 August 2012. They were placed in nearly the same highly elliptical, low-inclination orbits having a perigee of ~600 km altitude, an apogee of 5.8 R_E, and an inclination of 10°. The spacecraft spin at a rate of ~5 rpm and their spin axes point roughly sunward. The apogee is first located near 0800 magnetic local time (MLT) and precesses in local time westward at a rate of ~14 h/yr. The Van Allen Probes mission is described in more detail by *Mauk et al.* [2013].

2.2. EMFISIS/MAG and Waves

We use the magnetic field and plasma wave data obtained by the Electric and Magnetic Field Instrument Suite and Integrated Science (EMFISIS) instrumentation suite onboard the Van Allen Probes. EMFISIS provides two types of data sets: MAG and Waves. MAG consists of the magnetic field vector measured by a triaxial fluxgate magnetometer with a cadence of 64 Hz and a resolution of 0.16 nT/2 nT in ±4096 nT/±65536 nT range. Waves covers a wide frequency range of plasma waves. Wave signals in the frequency range of 10 Hz to 12 kHz are provided as vector electromagnetic fields, while those in the higher-frequency range of 10 kHz to 400 kHz are supplied with a single channel of the electric field. A more detailed description of EMFISIS can be found in the work by *Kletzing et al.* [2013].

The MAG data used in this study are averaged over 1 s (i.e., a cadence of 1 Hz) and are expressed in mean field-aligned (MFA) coordinates. A mean field is defined by a simple moving average of the magnetic field vector with a time window of 30 s, and its direction is taken to be the parallel direction in MFA coordinates. The radial direction is perpendicular to the mean field and points radially outward, and the azimuthal component is directed eastward to complete the right-handed system. We subtract the mean field from the observations to determine the magnetic field variations ($\Delta B_{\text{parallel}}$, ΔB_{radial}, and $\Delta B_{\text{azimuthal}}$) which are appropriate to examine ULF wave occurrence.

From the Waves measurements of plasma waves in the frequency range of 10–400 kHz, we search for the upper hybrid resonance band to determine the electron number density at a local probe position (n_{eL}). The determination of n_{eL} is made every 6 s with a semi-automated method, and is subjected to visual inspection and manual correction.

3. Observations of Oxygen Torus: 15 November 2012 Event

3.1. Orbits of Van Allen Probes

In this section, we focus on an observation of Probe A during 0330–1030 UT on 15 November 2012 and that of Probe B during 0420–1120 UT on the same day. Figure 1 illustrates these 7 h orbital segments of Probe A (red) and Probe B (blue) in solar magnetic (SM) coordinates. Small dots on the orbits indicate locations of probes at integer and half past hours. Both probes have almost the same trajectories starting from postmidnight and ending at the noon meridian via the dawn sector. Probe B tracks Probe A with a delay of approximately 50 min. In most of these intervals they are located below the geomagnetic equator.

3.2. Geomagnetic Conditions

Figure 2 shows the *AL*, *Wp*, and *Dst* indices for 11–16 November 2012. The *Wp* index reflects Pi2 wave power at low latitude on the nightside and is useful for identifying substorm onset [*Nosé et al.*, 2012]. The 7 h intervals of observations by Probe A and Probe B that are used in the present study are indicated by red and

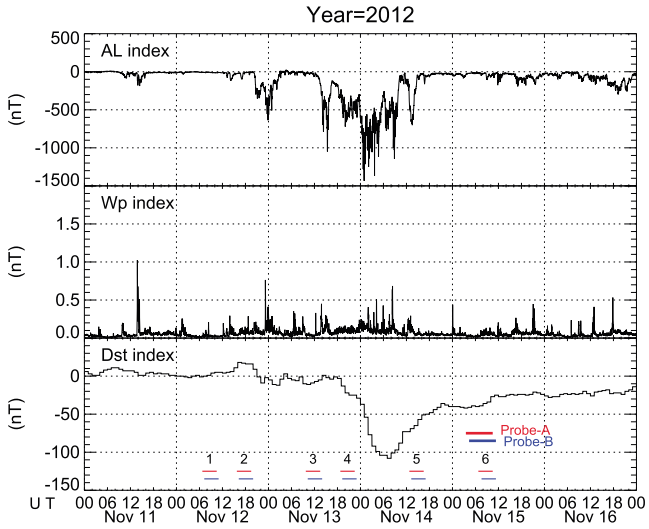

Figure 2. *AL*, *Wp*, and *Dst* indices for 11–16 November 2012. The 7 h intervals of observations by Probe A and Probe B are indicated by red and blue horizontal thick bars, respectively. Red and blue thin bars with numbers are time intervals discussed in section 4.

blue horizontal thick bars, respectively. (Red and blue thin bars with numbers are time intervals discussed in later section.) The observations are made during the recovery phase of the geomagnetic storm, in which the minimum value of the *Dst* index is −108 nT. The *AL* and *Wp* indices show that there are no major substorm activities during the probes observations.

3.3. EMFISIS Observations of ULF Waves

Figure 3a displays the EMFISIS data obtained by Probe A during 0330–1030 UT on 15 November 2012. The top three panels provide the dynamic power spectra of magnetic field perturbations in the ULF range of 0–50 mHz in MFA coordinates measured by EMFISIS/MAG. Figure 3a (bottom) shows the single axis frequency spectrogram of the electric field oscillation in the frequency range of 10–400 kHz measured by EMFISIS/Waves. In the top three panels, we identify ULF wave activities throughout the time interval with enhanced power after 0700 UT when the Probe A moves to the dayside. This is due to the enhanced

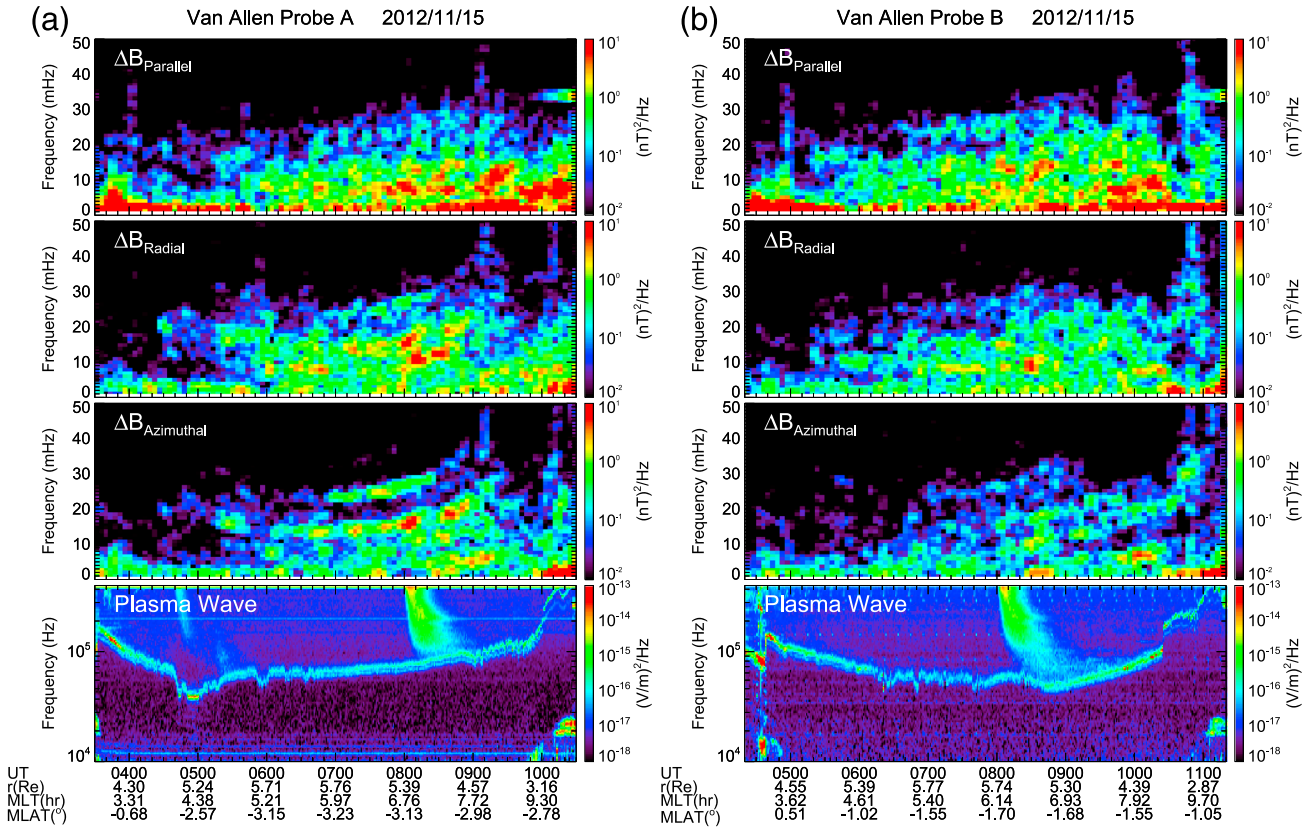

Figure 3. (a) EMFISIS data obtained by Probe A during 0330–1030 UT on 15 November 2012. (top three panels) The dynamic power spectra of magnetic field perturbations in the ULF range of 0–50 mHz in MFA coordinates measured by EMFISIS/MAG. (bottom) The single-axis frequency spectrogram of the electric field oscillation in the frequency range of 10–400 kHz measured by EMFISIS/Waves. (b) Same as Figure 3a but for Probe B during 0420–1120 UT on 15 November 2012.

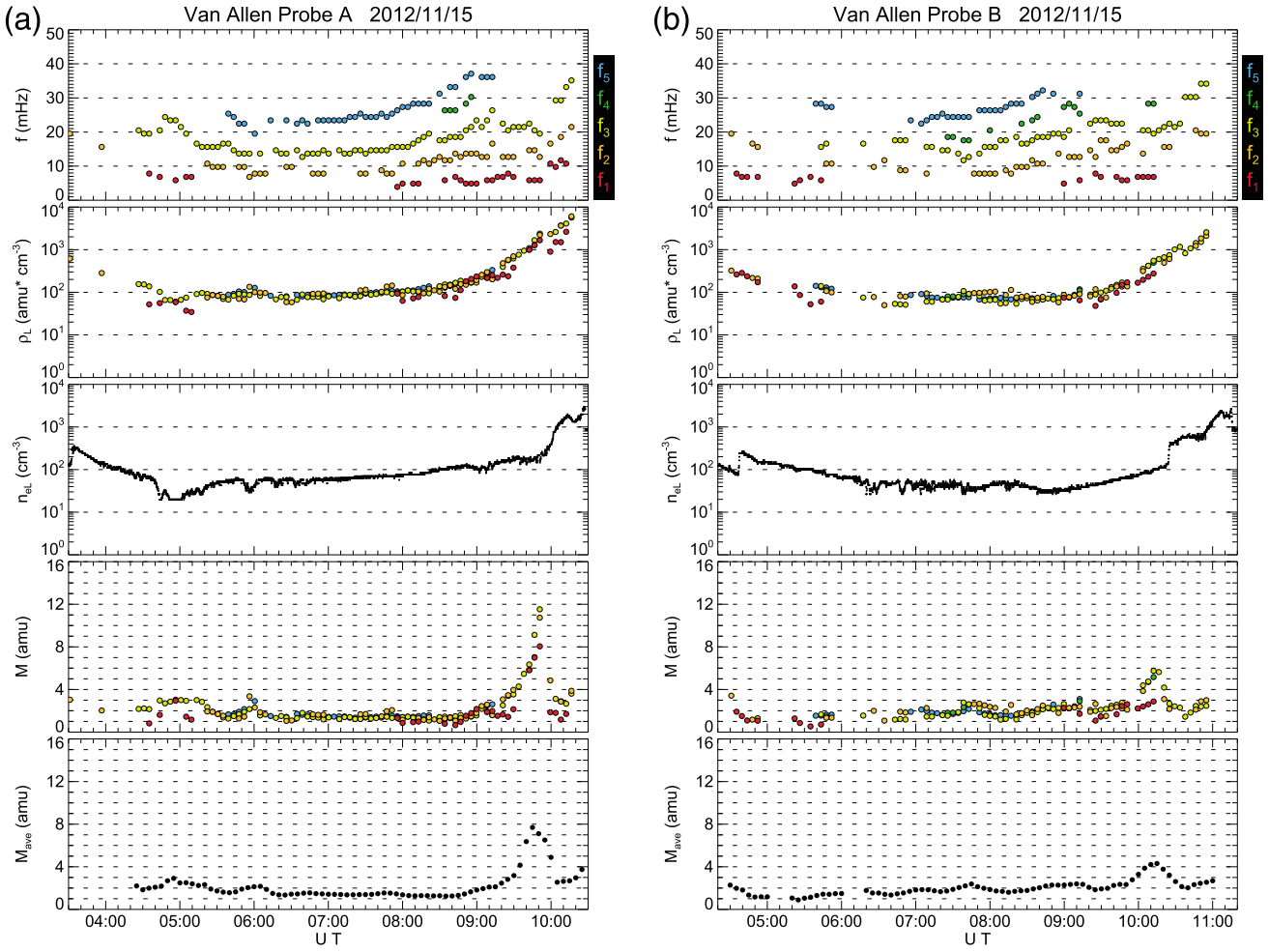

Figure 4. (a) Observational results from Probe A. From top to bottom: Selected harmonic frequencies (f_n), plasma mass density at a local probe position (ρ_L), electron number density at a local probe position (n_{eL}), average ion mass (M) derived from ρ_L and n_{eL} with the assumption of quasi-neutrality of plasma, and moving average of M with a time window of 20 min (M_{ave}). (b) Same as Figure 4a but for Probe B.

ionospheric conductivity on the dayside which creates effective reflection of the Alfvén waves and sets up a geomagnetic field line resonance. The harmonic structure of the field line resonance is most clearly visible in the azimuthal component. In Figure 3a (bottom), narrow banded upper hybrid resonance waves are clearly found.

Figure 3b is the same as Figure 3a but for Probe B. The similar features of ULF waves are identified in the top three panels. We also see a narrow band emission at the upper hybrid resonance frequency.

From the dynamic power spectrum of the azimuthal component, we select harmonic frequencies of the field line resonance to calculate the plasma mass density. First, the following criteria are used to select frequencies that have a local peak in wave power (f_p): (1) $P(f_p)/P(f_p - \Delta f) > 1.05$ and $P(f_p - \Delta f)/P(f_p - 2\Delta f) > 1.05$, (2) $P(f_p)/P(f_p + \Delta f) > 1.05$ and $P(f_p + \Delta f)/P(f_p + 2\Delta f) > 1.05$, and (3) $P(f_p) \geq 10^{-1.5}$ (nT^2/Hz), where $P(f)$ is the wave power at frequency f and Δf is the frequency resolution in the power spectrum. Because the power spectrum is calculated for data segments of 1024 data points, Δf is 0.98 mHz (1/1024 Hz). Second, the selected f_p is plotted over the dynamic power spectrum and is checked visually to discard values that do not match the harmonic structure. Finally, the harmonic number (n) is decided for each f_p. In this step, we consider that Probe A should observe the odd mode harmonics more clearly than the even mode harmonics because it was located off the equator (Figure 1). We also bear in mind that the third harmonic waves are often seen apparently off the equator, according to previous studies [e.g., *Takahashi et al.*, 2010]. We expect that Probe B tends to observe weaker odd mode waves and stronger even mode waves than Probe A, because Probe B flew closer to the geomagnetic equator. The electric field data

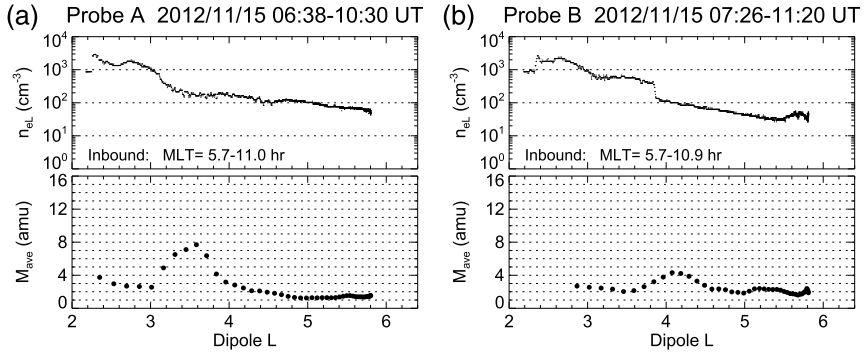

Figure 5. (a) The parameters n_{eL} and M_{ave} as a function of dipole L observed in the inbound pass of Probe A. (b) Same as Figure 5a but for Probe B.

[*Wygant et al.*, 2013] are also checked because it is useful to find the fundamental mode near the equator (not shown here). The selected harmonic frequencies are labeled f_n and are given in the top three panels of Figure 4a for Probe A and Figure 4b for Probe B. Colors represent the harmonic number from the fundamental ($n = 1$) to the fifth harmonics ($n = 5$).

3.4. Identification of Oxygen Torus

We estimate the plasma mass density at a local probe position (ρ_L) from f_n by numerically solving the MHD equation (1). The magnetic field is represented by the Tsyganenko 1989c (T89c) model [*Tsyganenko*, 1989] for $Kp = 1$; the first three values of the Kp index on 15 November 2012 are 1+, 1−, and 1−. The power law index of the ρ distribution in equation (2) is taken to be $\alpha = 0.5$. We take the ionospheric height of 200 km for both hemispheres, where $\xi = 0$. For each f_n, we decide on ρ_L which makes the field line resonance structure possess n antinodes. The results of estimation are shown in Figures 4a (second panel) and 4b (second panel). Different f_n gives the generally same values of ρ_L, indicating that the selection of f_n and the estimation of ρ_L are appropriate.

Figures 4a (third panel) and 4b (third panel) display n_{eL} calculated from the upper hybrid resonance band that are clearly identified in Figures 3a (bottom) and 3b (bottom). Probe A observes the plasmapause around 1000 UT at $r \sim 3.2\ R_E$ on the morning side (MLT ~9.3 h), and Probe B traverses the plasmapause around 1020 UT at $r \sim 4.0\ R_E$ and MLT ~ 8.4 h. This is due to expansion of the plasmasphere during the storm recovery phase, which can be recognized more easily in later figures (Figures 5 and 6). On the nightside, although some plasma depletion regions are noted (e.g., 0440–0530 UT, around 0600 UT for Probe A, and 0400–0420 UT, 0610–0650 UT for Probe B), n_{eL} changes rather smoothly and no clear plasmapause is detected. Such a smooth transition of n_{eL} from the plasmasphere to the plasma trough without a clear signature of the plasmapause and its preference to quiet geomagnetic conditions have been reported by *Moldwin et al.* [2002] and *Tu et al.* [2007].

The next panels of Figures 4a and 4b display M derived from ρ_L and n_{eL} with the assumption of quasi-neutrality of plasma. Calculation is made by using the data shown in the second and third panels. We have a reasonable estimation of M ranging from 1 amu to 12 amu. Even if the harmonics are different, the estimated values of M generally coincide with each other. In order to increase statistical significance, we compute the moving average of M with a time window of 20 min. If no more than two values of M are included in the 20 min window, no average is computed. The results (M_{ave}) are demonstrated in Figures 4a (bottom) and 4b (bottom). Both observations of Probe A and Probe B show that M_{ave} is 1–2 amu in the plasma trough. A subtle enhancement of M_{ave} (~3 amu) is noted around 0500 UT for Probe A. However, the most distinct enhancements appear at 0930–1000 UT for Probe A and at 1000–1030 UT for Probe B when both Probes are located around MLT = 8–9 h. Their peak values are 4.5–8 amu, which means the O^+ concentration to be 23–47% if the plasma is composed of only H^+ and O^+. These enhancements are identified just outside of or very close to the plasmapause. This feature is consistent with that of the oxygen torus reported by previous studies [*Chappell*, 1982; *Horwitz et al.*, 1986; *Takahashi et al.*, 2008; *Nosé et al.*, 2011]. We cannot investigate the presence of the oxygen torus in other MLT during this specific magnetic storm due to the Van Allen Probes orbits, though the O^+ density enhancements have been reported at local times other than the morning side [e.g., *Horwitz et al.*, 1984, 1986; *Roberts et al.*, 1987].

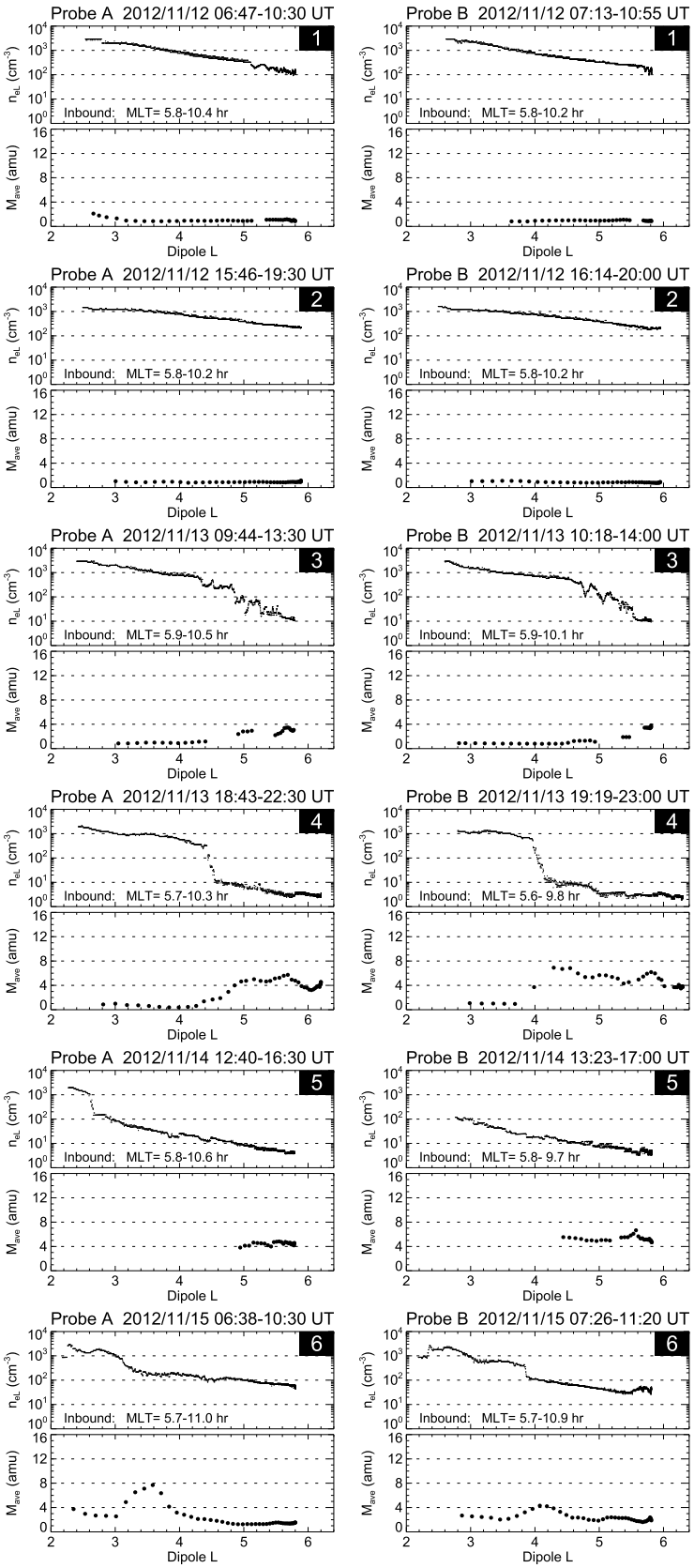

Figure 6. The parameters n_{eL} and M_{ave} as a function of dipole L observed by (left column) Probe A and (right column) Probe B during time intervals 1–6 indicated in Figure 2.

The same data of n_{eL} and M_{ave} are plotted as a function of dipole L in Figure 5. Only inbound observations are shown, because the oxygen torus is found on the morning side (MLT ~ 8–9 h). We determine from the Probe A observation (Figure 5a) that the plasmapause is located at $L \sim 3.2$ and the oxygen torus is distributed over $L = 3.0$–4.0. Probe B detects the plasmapause at $L \sim 3.9$ and the oxygen torus at $L = 3.7$–4.5 (Figure 5b). *Roberts et al.* [1987] introduced an empirical equation between the L shell of the O^+ density peak and the Kp index: $L = -0.24\,Kp + 4.39$. If we substitute $Kp = 1$ in this equation, we obtain $L = 4.15$ for the O^+ peak location, which is consistent with the Probe B observation.

4. Observations of Oxygen Torus Formation

We derive M on the morning side before 15 November 2012 to investigate the evolution of the oxygen torus. The magnetic field data from Van Allen Probes are visually scanned for 12–14 November 2012 to find clear ULF signatures. For both Probe A and Probe B, we find five orbital segments on the morning side, in which clear harmonic structures appear in a dynamic power spectrum. The time intervals of these five orbital segments are indicated in Figure 2 with red (Probe A) and blue (Probe B) horizontal thin bars labeled 1–5. We also indicate with thin bars labeled 6 the time intervals examined in Figure 5, during which the oxygen torus is identified. Intervals 1 and 2 are during the quiet period or sudden commencement. Interval 3 is the initial phase of the magnetic storm. Intervals 4 and 5 are during the main phase and the early recovery phase of the magnetic storm, respectively. The trajectories of Van Allen Probes during these five intervals are nearly identical to the inbound path in the morning sector shown in Figure 1.

We perform an analysis similar to that used in the section 3 for the EMFISIS data during the five time intervals. Figure 6 displays the results of estimation of n_{eL} and M_{ave} as a function of dipole L for intervals 1–5 as well as interval 6; results for interval 6 are the same as those in Figure 5. The left column shows the results of Probe A, and the right column shows those of Probe B. Before the magnetic storm starts (intervals 1 and 2), both probes stay inside the plasmasphere and measure 100% H^+ plasma. In the initial phase (interval 3), the plasmasphere starts to shrink and both probes encounter gradual decreases of n_{eL} over $L = 4.5$–5.8. The plasma in the plasmasphere at $L < 4.5$ has $M_{ave} \sim 1$ amu, whereas that in the plasmapause or plasma trough shows enhancement of M_{ave} up to 4 amu. This indicates that heavy ions (He^+ and O^+) with thermal energy are loaded in the magnetosphere already in the initial phase, although the *Dst* index is not fully decreased yet. During the storm main phase (interval 4), a clear plasmapause is identified near $L = 4.3$ with Probe A and near $L = 4.1$ with Probe B, resulting from shrinkage of the plasmasphere during the storm development. M_{ave} still remains at about 1 amu in the plasmasphere, but it is increased to 4–7 amu in the plasma trough. A closer comparison of the two panels in interval 4 reveals that M_{ave} becomes larger during the time interval between the Probe A and Probe B observations, in particular, at $L = 4$–5. We consider that this is due to the continuous loading of heavy ions to the plasma trough and that the heavy ions should be mostly O^+ ions because M_{ave} is larger than 4 amu. In the early recovery phase (interval 5), Probe A detects the plasmapause at $L = 2.6$. There are no ULF activities at $L < 5$ during this interval and no information about M_{ave} is obtained. However, M_{ave} in the plasma trough at $L = 5$–5.8 is nearly constant at 4–5 amu, which is similar to that in interval 4. We therefore suppose that such a large value of M_{ave} prevails down to the plasmapause. Probe B also detects ULF activity at only $L = 4.4$–5.8, where M_{ave} is estimated to be 5–7 amu and shows a small enhancement in comparison with the Probe A observation (i.e., 4–5 amu). We have the same supposition that the plasma trough has a large M_{ave} (~4–7 amu) throughout, while the plasmasphere has $M_{ave} \sim 1$ amu. Finally, in the late recovery phase (interval 6), we find the oxygen torus near the plasmapause.

5. Discussion

5.1. Generation Mechanisms of Oxygen Torus

Two scenarios have been proposed for the formation of the oxygen torus: (1) ionospheric electron heating scenario and (2) geomagnetic mass spectrometer scenario [e.g., *Roberts et al.*, 1987]. The first scenario considers interactions between the ring current energetic ions and the plasmaspheric cold electrons during the recovery phase because of the expansion of the plasmasphere. One of the possible interactions is Coulomb collision as an energy transfer process from the ring current protons to the plasmaspheric cold electrons [*Cole*, 1965]. Another possible interaction is Landau damping of ion cyclotron waves that are generated by unstable ring current ions and consequent heating of the plasmaspheric electrons [*Cornwall et al.*, 1971]. In either interaction, the plasmaspheric cold electrons are energized, and the heat conduction from the plasmaspheric electrons down to the underlying ionosphere becomes responsible for a rise of the

temperature in the ionospheric ions. This results in an increase of the scale height of ionospheric plasma and extraction of a large number of O^+ ions into the high altitude. Then the oxygen torus is formed in the limited *L* shell where the ring current and the plasmasphere interacted [*Roberts et al.*, 1987, Figure 17].

In the second scenario, ionospheric ions are extracted from a region near the dayside polar cusp during the initial or main phase of magnetic storms and are convected into the nightside polar cap region. Because of the polar convective electric field, the ionospheric ions are subsequently transported into the magnetosphere or the plasma sheet by the E × B drift. The E × B drift velocity is the same for all ions, but heavier ions have a smaller tailward velocity than lighter ions if escaping energies from the ionosphere are the same. This makes mass spectrometer effect such that heavier ions fall in the near-Earth magnetosphere while lighter ions are transported farther tailward. Because the extracted O^+ ions reach the near-Earth magnetosphere in a time scale of several hours [*Cladis*, 1986, 1988], an area with high concentration of the ionospheric O^+ ions is formed outside the plasmasphere during the storm main phase. Then the plasmapause expands during the storm recovery phase and some parts of the ionospheric O^+ ions in the near-Earth magnetosphere are trapped within the plasmapause, resulting in formation of the oxygen torus [*Roberts et al.*, 1987, Figure 16].

Analyzing simultaneous and conjugate measurements of the DE 1 and DE 2 satellites, *Horwitz et al.* [1986] reported that O^+ density enhancements in the plasmasphere are often closely coincident with ionospheric electron temperature enhancements and concluded that the first scenario is plausible. The same conclusion has been derived by *Roberts et al.* [1987], *Comfort et al.* [1988], and *Horwitz et al.* [1990]. However, we find loading of thermal heavy ions in the whole plasma trough at $L < 5.8$ in the initial and main phases of the magnetic storm on 13–14 November 2012 (intervals 3–5 in Figure 6). This observational result appears to favor the second scenario rather than the first scenario. Moreover, the magnetic storm examined in the present study started with a sudden commencement (Figure 1). In such magnetic storms, a large amount of O^+ ions are extracted from the cusp region when the solar wind dynamic pressure is enhanced [*Moore et al.*, 1999, 2001; *Elliott et al.*, 2001; *Kunori et al.*, 2007], which is also supportive of the second scenario.

5.2. Numerical Calculation of Thermal O^+ Ion Trajectories

5.2.1. Temporal Evolution of O^+ Ion Distribution During Storm Recovery

In the second-generation mechanism, it is considered that the ionospheric O^+ ions prevailing in the plasma trough are trapped in the expanding plasmasphere during the recovery phase to form the oxygen torus. This process is examined here with numerical calculation. A dipole magnetic field and the Volland-Stern convection electric field [*Volland*, 1973; *Stern*, 1975; *Maynard and Chen*, 1975] are assumed. The convection field potential Φ is determined by

$$\Phi = \frac{0.045}{(1 - 0.159\,Kp + 0.0093\,Kp^2)^3} r^2 \sin\left(\pi \frac{\mathrm{LT}}{12}\right), \tag{4}$$

where *r* is a radial distance. To simulate recovery of a magnetic storm, the *Kp* index is changed as $Kp = -t/6 + 3$ (t = 0–12 h) and $Kp = 1$ ($t > 12$ h), where *t* is an elapsed time and t = 0–15 h. At $t = 0$ h, we put equatorial mirroring thermal O^+ ions only in the plasma trough at $(X, Y) = (-8$ to 8 R_E, -8 to 8 $R_E)$ with a grid spacing of 0.5 R_E. This is because we observe heavy ions outside the plasmapause in the storm main phase (interval 4). Thermal energies of the O^+ ions are taken to be 15 eV, 50 eV, 100 eV, 300 eV, and 1000 eV. We then calculate the trajectories of the O^+ ions under the decreasing convection electric field. No O^+ ions are added during $t > 0$ h, which reflects in a very simple manner a cessation or a decrease of the O^+ supply from the dayside polar cusp during the storm recovery phase. The results of the calculation are shown in Figure 7. Each panel displays the positions of the O^+ ions (small dots) and an open/closed separatrix for cold ions (a thick curve) that is considered the plasmapause at t = 0, 3, 4.5, 6, 7.5, 9, 10.5, 12, and 15 h. Colors of the small dots represent initial energies of the O^+ ions (i.e., from 15 eV to 1000 eV) as indicated in the legend. Most of O^+ ions drift eastward because of their low energy. At t = 3–4.5 h, the O^+ ions drape around the plasmapause on the nightside, while they are also found in a wider range of *r* on the dayside. In the morning sector, the O^+ ions are distributed from the plasmapause up to $r \sim 7$–8 R_E. At t = 6–9 h, the O^+ ions further drift eastward to the dayside in the vicinity of the plasmapause. As the *Kp* index gradually decreases, the plasmapause correspondingly expands. Some of the O^+ ions are then found inside the open/closed separatrix, having been trapped within the plasmasphere. These processes create regions where the O^+ ions are concentrated both outside and inside the plasmasphere. The regions extend over a radial width of 1–2 R_E on the dawn and morning sides. At $t = 12$ h, the plasmapause has fully expanded. The O^+ ions mostly remain in a limited range of *r* within the plasmasphere. As time proceeds ($t = 15$ h), the trapped O^+ ions in

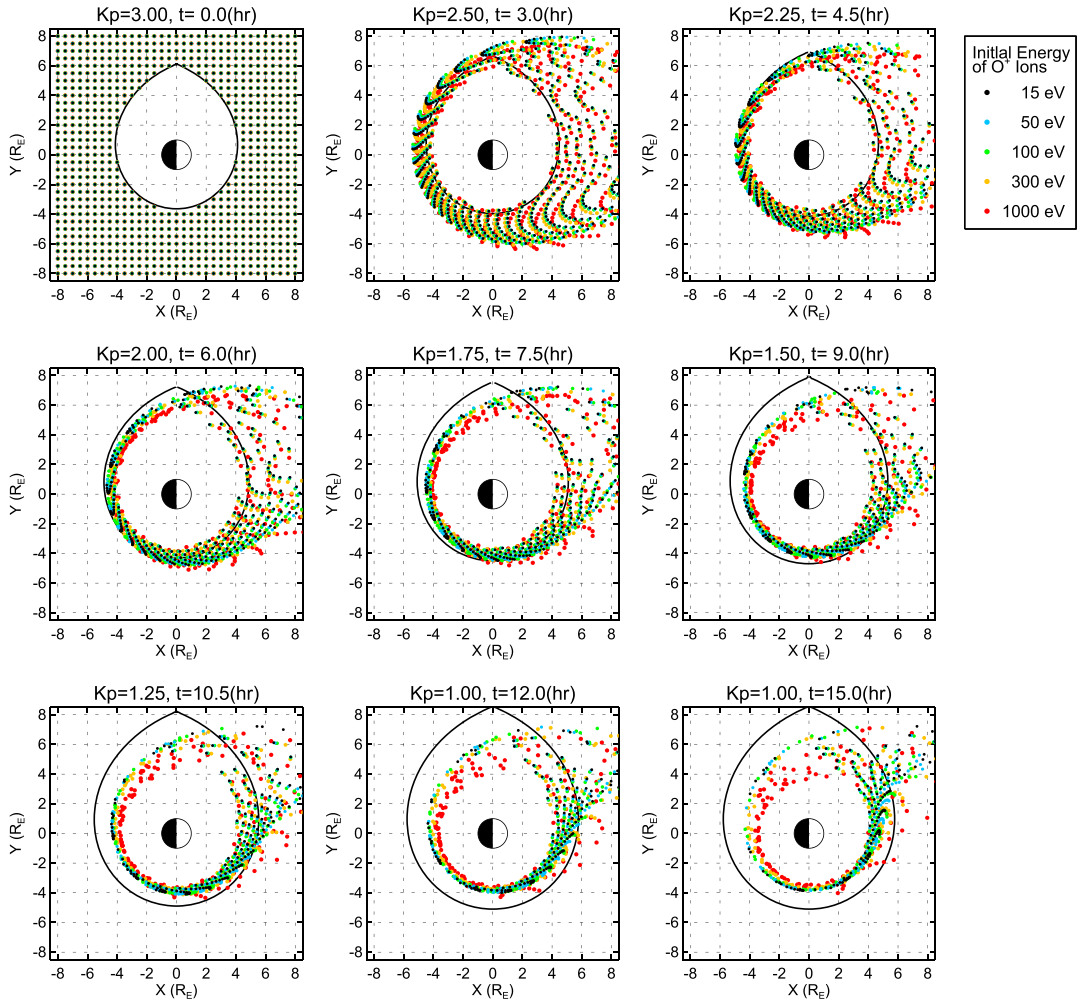

Figure 7. Results of numerical calculation of O^+ ion drift during a decrease of the convection electric field. A dipole magnetic field and the Volland-Stern convection electric field are assumed at $t = 0$ h, equatorial mirroring O^+ ions with energies of 15 eV, 50 eV, 100 eV, 300 eV, and 1000 eV are put only in the plasma trough at $(X, Y) = (-8$ to 8 R_E, -8 to 8 $R_E)$ with a grid spacing of 0.5 R_E. The Kp index is changed as $Kp = -t/6 + 3$ ($t = 0$–12 h) and $Kp = 1$ ($t > 12$ h). A thick curve represents an open/closed separatrix, for cold ions, that is considered the plasmapause.

the plasmasphere corotate eastward with the Earth at $r \sim 4$–6 R_E. The present numerical calculation indicates that O^+ ions are not only trapped within the plasmasphere but also draped around the plasmapause on the dawn and morning sides during the recovery phase, forming an oxygen torus that exists from just inside the plasmasphere and protrudes outward from the plasmapause.

5.2.2. Comparison With Van Allen Probes Observations

In order to compare with the Van Allen Probes observations, we examinethe O^+ ion density on the morning side as a function of radial distance by using the results of the numerical calculation. The O^+ density here is defined by the number of O^+ ions divided by an area, each of which covers 8–11 h of local time by 0.5 R_E of r. Figure 8 shows results for $t = 0$, 3, 4.5, 6, 7.5, 9, 10.5, and 12 h (i.e., during the plasmapause expansion), which are differentiated by colors as specified. Stars represent the plasmapause positions averaged over 8–11 h in local time. The O^+ density in the plasma trough is rather uniform at $t = 0$ h, as is expected for the initial condition. The O^+ density at $t = 3$ h is generally lower, likely because the ions have drifted into the dayside. In the following intervals at $t = 4.5$–6 h, the density at $r = 3.5$–6 R_E reverts to or becomes larger than the

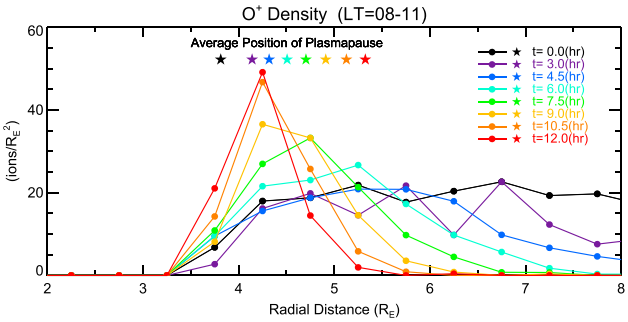

Figure 8. O^+ ion density on the morning side as a function of radial distance at t = 0, 3, 4.5, 6, 7.5, 9, 10.5, and 12 h (i.e., during the plasmapause expansion). The O^+ density is defined by the number of O^+ ions divided by an area, each of which covers 8–11 h of local time by 0.5 R_E of r. Stars represent the plasmapause positions averaged over 8–11 h in local time.

initial values. We ascribe these density changes to ions that drift eastward from the nightside. These simulation results are consistent with the Van Allen Probes observations in interval 5, where the small enhancement of M_{ave} from 4–5 amu to 5–7 amu is detected at L = 5–5.8 during the time interval between the Probe A and Probe B measurements (Figure 6).

At t = 7.5 h, a clear peak occurs in the O^+ density at r = 4.5–5 R_E with a peak value about 1.5 times that of the previous values. The density peak is located near the plasmapause. This is because ions originating from the nightside corotate eastward around the plasmapause and have approximately the same trajectories on the morning side, as shown in Figure 7. This simulation result agrees well with the Probe A observation at interval 6, where M_{ave} shows a peak of ~8 amu near the plasmapause (Figure 6). The density peak moves inward at t = 9 h, while the plasmapause expands to r = 4.9 R_E. This puts the O^+ density peak within the plasmasphere where cold and dense H^+ ions are expected. We suppose that this O^+ density peak is not distinctly identified from the Van Allen Probes observations of M_{ave}, because the dense plasmaspheric H^+ ions make M_{ave} values smaller. Outside the plasmasphere (r > 5 R_E), the O^+ density becomes lower than that at t = 7.5 h. Thus, we expect that M_{ave} may show a broad peak around the plasmapause with a value lower than previously observed by Probe A at interval 6. The above supposition appears to be consistent with the Probe B observation of M_{ave} in interval 6 where the plasmapause is located at L ~ 3.9 and the oxygen torus is distributed over L = 3.7–4.5 with the peak value of ~4 amu (Figure 6).

Near the end of the plasmapause expansion at t = 10.5–12 h, the O^+ density exhibits a distinct peak at r = 4–4.5 R_E located well within the plasmasphere. Similarly, we speculate that the density peak is not distinctly visible in M_{ave} because of the dense plasmaspheric H^+ ions, although no observations of M_{ave} are made after interval 6 in the present study.

5.2.3. Validity of Initial Parameters of O^+ Ions

In the numerical calculation we consider O^+ ions with a pitch angle (α_{pitch}) of 90° and thermal energies of 15 eV, 50 eV, 100 eV, 300 eV, and 1000 eV, at t = 0 h (i.e., at the beginning of the storm recovery phase). Here we discuss whether these initial parameters of the O^+ ions are appropriate.

Calculating the guiding center motion of ions, *Cladis* [1986] showed that O^+ ions starting near the dayside polar cusp with an energy of ~12 eV arrive in the nightside magnetosphere at r = 8 to 15 R_E with final energies of 400 eV to a few keV. The transit time of the O^+ ions from the dayside polar cusp to the magnetosphere was found to be 1–2 h, which was also reported by *Cladis and Francis* [1992]. A thorough examination about destination of outflowing ionospheric O^+ ions was performed by *Ebihara et al.* [2006]. They calculated the trajectories of O^+ ions that are launched with energies of <209 eV from the polar ionosphere covering 50°–90° of magnetic latitude and the entire MLT. It was found that the ring current at L = 5 is the most common destination of O^+ ions launched from the polar region (>70° magnetic latitude). The O^+ ion with an initial energy of 14 eV arrives at L = 5 during a transit time of 2.8 h. The simulated ion flux of O^+ ions at L = 5 has multicomponents such as thermal (1 eV to ~100 eV), suprathermal (~100 eV to 10 keV), and energetic (10–70 keV), with the prevalence of the thermal component [*Ebihara et al.*, 2006, Figure 8]. Therefore, we consider that the initial energies of O^+ ions used in the present numerical calculation are quite reasonable. The transit time of O^+ ions reported by the previous studies is a few hours, which is shorter than the time scale of the storm main phase, implying that thermal O^+ ions have been supplied from the ionosphere into the plasma trough before the recovery phase begins. We also consider that it is reasonable to place the thermal O^+ ions in the plasma trough at the beginning of the recovery phase.

It is expected that thermal O^+ ions are energized by the drift-betatron acceleration when they drift inward from the near-Earth plasma sheet to the inner magnetosphere under the influence of the convective electric

field. This creates a pitch angle distribution of O^+ ions with a peak flux around $\alpha_{pitch} = 90°$ (i.e., pancake distribution). Thus, it is not unrealistic to consider only equatorial mirroring O^+ ions ($\alpha_{pitch} = 90°$) in the numerical calculation, although in the actual magnetosphere a smaller amount of O^+ ions having velocity in the direction parallel to the magnetic field ($\alpha_{pitch} \neq 90°$) would be present.

5.3. Comparison Between Oxygen Torus and Warm Plasma Cloak

Chappell et al. [2008] shed new light on a plasma population with energies of 10 eV–3 keV in the inner magnetosphere, compiling satellite measurements of low-energy ions over the past 30 years and conducting a statistical analysis of the thermal ion fluxes at <400 eV measured by the Polar satellite. This low-energy plasma population was called the "warm plasma cloak," because it was draped over the nightside region of the plasmasphere and spread out to higher L shells in the morning and early afternoon sectors. In order to examine the source and evolution of warm plasma cloak ions, *Chappell et al.* [2008] calculated the trajectories of polar wind ions in a three-dimensional steady state magnetosphere expressed by the T89c magnetic field model and the Volland-Stern electric field model. All ions that form the warm plasma cloak were found to have a nightside equatorial crossing distance from 8 to 45 R_E geocentric and never exceed about 3 keV in energy. From recent observations by the Time History of Events and Macroscale Interactions during Substorms (THEMIS) spacecraft, *Lee and Angelopoulos* [2014] identified the warm plasma cloak wrapping around the dawnside with temperatures from ~10 eV (H^+), tens of eV (He^+), to hundreds of eV (O^+). We note that the morphology and location of the oxygen torus shown in Figure 7 are nearly identical to those of the warm plasma cloak discussed by *Chappell et al.* [2008] and *Lee and Angelopoulos* [2014]. In our calculation, however, the O^+ density enhancement can be created just inside the plasmapause because of a temporal change in the convection electric field, whereas *Chappell et al.* [2008] argued that the warm plasma cloak is distributed only outside the plasmapause.

The enhancement of O^+ density in a limited range of L shell has been referred to as the oxygen torus, which implies revolution symmetry. However, the results of the present numerical calculation (Figure 7) and schematic figures of the warm plasma cloak [*Chappell et al.*, 2008, Figures 3, 15, and 16] suggest a crescent-shaped torus or a pinched torus that is centered around the dawn or midmorning sectors and spans the sectors from premidnight to early afternoon. The oxygen-pinched torus can explain the high-occurrence frequency (≥70%) of the O^+ enhancement in the late evening and dawn regions (20–24 MLT and 05–09 MLT) reported by *Roberts et al.* [1987].

5.4. ECT-HOPE Observations

The Van Allen Probes carry the Helium, Oxygen, Proton, and Electron (HOPE) mass spectrometers which are one of the three pairs of instruments of the Energetic Particle, Composition, and Thermal Plasma (ECT) suite. The HOPE instruments are designed to measure the in situ ion fluxes over 4π sr with the energy range from 1 eV to 50 keV and with mass and charge state information [*Funsten et al.*, 2013]. It is of great interest to examine what the HOPE instruments observed while the oxygen torus was identified in the recovery phase of the November 2012 storm (interval 6).

For an easier comparison with the HOPE data, we again demonstrate n_{eL} and M_{ave} as a function of dipole L during interval 6 in Figure 9a (Probe A) and Figure 9b (Probe B), which are identical to Figure 5. The plasmapause is identified at $L = 3.2$ in Figure 9a and at $L = 3.9$ in Figure 9b as indicated by vertical dashed lines. We calculated HOPE ion moments over the energy range of 30 eV–1 keV, where the lower energy limit of 30 eV is determined to avoid possible errors from spacecraft charging effects and the upper energy limit of 1 keV is determined to exclude contribution from energetic ring current ions. It is known that the computed densities of H^+, He^+, and O^+ reflect only a portion of cold plasma density, that is, only the population at >30 eV. We therefore refer to the computed density as partial density. In Figures 9c and 9d, we display the partial densities of H^+ (red, n_{pH^+}), He^+ (yellow, n_{pHe^+}), and O^+ (green, n_{pO^+}) as a function of dipole L for Probe A and Probe B, respectively. Furthermore, we indicate the sum of these partial densities ($n_{pH^+}+n_{pHe^+}+n_{pO^+}$) with a black line. Vertical dashed lines represent the locations of the plasmapause indicated in Figures 9a and 9b. The sum of the partial densities in the plasma trough is 0.5–1 cm^{-3} as shown in Figures 9c and 9d, which is significantly lower than the ion densities of 20–200 cm^{-3} inferred from n_{eL} (Figures 9a and 9b) by assuming the quasi-neutrality of plasma. This suggests that ions with energies lower than 30 eV predominantly contribute to the ion density. In the plasmasphere, the discrepancy between the sum of the partial densities (0.002–2 cm^{-3}) and the ion density inferred from n_{eL} (500–2000 cm^{-3}) becomes even larger,

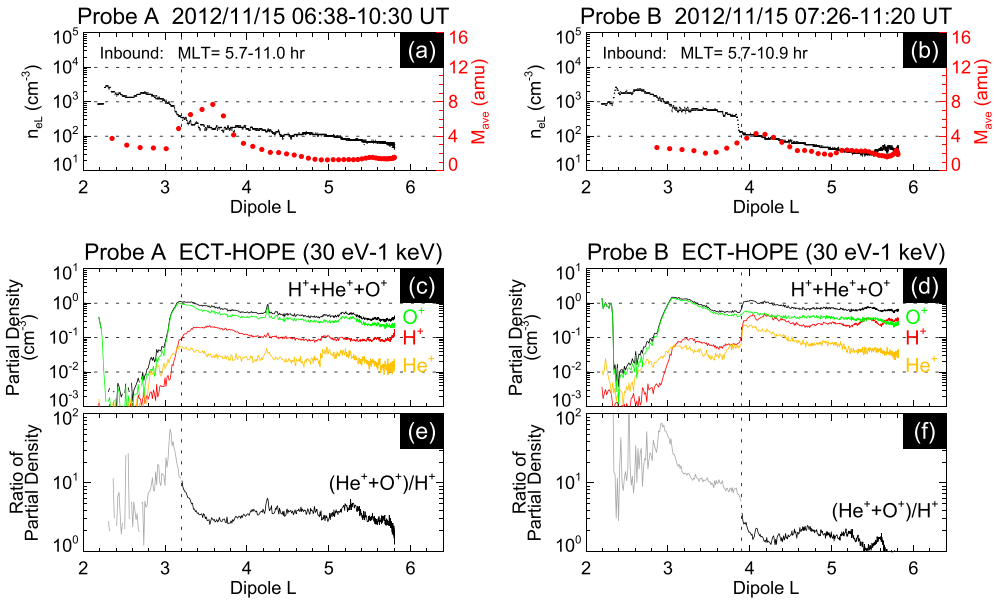

Figure 9. (a) The parameters n_{eL} (black) and M_{ave} (red) as a function of dipole L observed by Probe A in interval 6. (b) Same as Figure 9a but for Probe B. (c) Partial densities of H^+ (red), He^+ (yellow), and O^+ (green) measured by the HOPE instrument as a function of dipole L for Probe A in interval 6. The partial densities are calculated over the energy range of 30 eV–1 keV. The sum of these partial densities is shown with a black line. (d) Same as Figure 9c but for Probe B. (e) Partial density ratio of heavy ions (He^+ and O^+) relative to H^+ as a function of dipole L for Probe A. The ratio in the plasmasphere is plotted with a gray line, because of the small and unrealistic value of the H^+ partial density. (f) Same as Figure 9e but for Probe B.

because ions with energies of <30 eV occur to a greater extent in the plasmasphere than in the plasma trough [*Goldstein et al.*, 2014].

In spite of such limitation of the partial densities computed over 30 eV–1 keV, they may still provide some insights about ion composition. Figure 9c shows that n_{pO^+} predominantly contributes to the sum of the partial densities. The partial densities in the plasma trough are almost constant or increase gradually as the probe moves inward down to the plasmapause. A closer inspection reveals distinct enhancements of n_{pO^+} and n_{pHe^+} immediately outside the plasmapause (L = 3.2–3.4) where no such enhancements are identified in n_{pH^+}. In the plasmasphere, all of the partial densities fall to <0.1 cm^{-3}; we refrain from discussing the ion composition with the possibly uncertain data. Figure 9d shows the similar signatures of the ion composition in the plasma trough (L > 3.9). There are also enhancements in n_{pO^+} and n_{pHe^+} outside the plasmapause (L = 3.9–4.2). In the plasmasphere at L = 3–3.9, Probe B observed the partial densities of 0.02–1.5 cm^{-3}, which are larger than the plasmaspheric partial densities observed by Probe A (Figure 9c), in particular, for O^+ ions. This may have occurred because plasma that resided in the plasma trough are trapped inside the plasmasphere during the expansion of the plasmapause, as shown in Figure 7.

In order to confirm the density enhancements of O^+ and He^+ relative to H^+ just outside the plasmapause, we calculate a ratio of the partial densities such as $(n_{pHe^+} + n_{pO^+})/n_{pH^+}$; the results are shown in Figure 9e (Probe A) and Figure 9f (Probe B). The ratio in the plasmasphere is plotted with a gray line and will not be discussed further, because of the very small and unrealistic values of n_{pH^+}. We note that the ratio of the partial density is enhanced near the plasmapause at L = 3.2–3.4 in Figure 9e and at L = 3.9–4.2 in Figure 9f. It is, however, difficult to quantitatively compare these enhancements of the partial density ratio (Figures 9e and 9f) with the enhancements of M_{ave} (Figures 9a and 9b), because the partial densities are calculated over 30 eV–1 keV that is out of the energy range for cold ions contributing to M_{ave}. Nevertheless, it is supposed that the enhancements of the partial density ratio may have some connection with the oxygen torus in regard to their characteristics that they are located outside the plasmapause and limited in a narrow L range.

6. Conclusions

We have identified the oxygen torus using the magnetic field and plasma wave data obtained by the Van Allen Probes during the 12–15 November 2012 magnetic storm and have examined its formation process. Both Probe A and Probe B observe the oxygen torus on the morning side (MLT ~ 8–10 h) at L = 3.0–4.0 and L = 3.7–4.5 during the storm recovery phase. The average plasma mass in the torus is estimated to be 4.5–8 amu, which indicates that the O^+ concentration is 23–47% if the plasma is composed of only H^+ and O^+. The plasmapause is found at L ~ 3.2 and 3.9 by Probe A and Probe B, respectively. Thus, the oxygen torus is located near the plasmapause and extends over both the plasmasphere and the plasma trough.

We perform similar analysis for data obtained during the quiet period, the initial phase, and the main phase. During the quiet period, the average plasma mass is near 1 amu in the plasmasphere. In the following periods, the average plasma mass is 4–7 amu throughout the plasma trough and remains at ~1 amu in the plasmasphere. These results imply that ionospheric O^+ ions are supplied into the inner magnetosphere already in the initial phase of the magnetic storm, though the *Dst* index is not yet fully decreased. Previous studies reported that a large amount of O^+ ions are extracted from the cusp region when the solar wind dynamic pressure is enhanced and they contribute to the plasma in the near-Earth plasma sheet or the ring current region. The 12–15 November 2012 magnetic storm initiated with a sudden commencement and supports the above implication.

Numerical calculation is performed to investigate whether the thermal O^+ ions distributed in the plasma trough form the oxygen torus during the decrease of the convection electric field. It is found that some of the O^+ ions are trapped within the expanded plasmasphere, while some of them drift around the plasmapause on the dawnside. The numerical results demonstrate how the oxygen torus spreads around the plasmapause and are consistent with the Van Allen Probes observations. The oxygen torus identified in this study favors the formation scenario of the geomagnetic mass spectrometer and the O^+ drift during the recovery phase (scenario 2 in section 5.1). We do not, however, rule out the other formation scenario due to ionospheric electron heating (scenario 1 in section 5.1). If magnetic storms start without a sudden commencement or if the oxygen torus is confined within the plasmasphere as shown by *Horwitz et al.* [1986], scenario 1 may be more plausible.

The present numerical calculations and previous studies reporting on the warm plasma cloak [*Chappell et al.*, 2008; *Lee and Angelopoulos*, 2014] suggest that a crescent-shaped torus or a pinched torus centered around the dawnside better describes the longitudinal extent of the O^+ density enhancement.

Acknowledgments

The *AL* and *Dst* indices were provided by the World Data Center for Geomagnetism, Kyoto, and are available at http://wdc.kugi.kyoto-u.ac.jp. The *Kp* index was provided by H. J. Linthe at the Helmholtz Centre Potsdam, GFZ German Research Centre for Geosciences and is available at http://www.gfz-potsdam.de/kp-index. The *Wp* index can be downloaded from http://s-cubed.info. The EMFISIS data are available at http://emfisis.physics.uiowa.edu. The ECT-HOPE data are available at http://www.rbsp-ect.lanl.gov. The electron number density at a local probe position can be obtained on request from W. S. Kurth (william-kurth@uiowa.edu). Geomagnetic field by the Tsyganenko 1989c model was calculated with GEOPACK routines developed by N. A. Tsyganenko and coded by H. Korth. We are thankful to K. Takahashi, and Y. Obana for their helpful comments. This study was supported by the Ministry of Education, Culture, Sports, Science and Technology (MEXT), grant-in-aid for Scientific Research (B) (grant 25287127). The work at Iowa was supported by JHU/APL contract 921648 under NASA Prime contract NAS5-01072. This work was supported by RBSP-ECT funding provided by JHU/APL contract 967399 under NASA Prime contract NAS5-01072. Work at Los Alamos National Laboratory was performed under the auspices of the U.S. Department of Energy, LA-UR-15-20090. Part of the work by one of coauthors (KK) has been done at the ERG-Science Center operated by ISAS/JAXA and STEL/Nagoya University.

Michael Liemohn thanks the reviewers for their assistance in evaluating this paper.

References

Chappell, C. R. (1982), Initial observations of thermal plasma composition and energetics from Dynamics Explorer-1, *Geophys. Res. Lett.*, *9*, 929–932, doi:10.1029/GL009i009p00929.

Chappell, C. R., S. A. Fields, C. R. Baugher, J. H. Hoffman, W. B. Hanson, W. W. Wright, H. D. Hammack, G. R. Carignan, and A. F. Nagy (1981), The retarding ion mass spectrometer on dynamics explorer-A, *Space Sci. Instrum.*, *5*, 477–491.

Chappell, C. R., M. M. Huddleston, T. E. Moore, B. L. Giles, and D. C. Delcourt (2008), Observations of the warm plasma cloak and an explanation of its formation in the magnetosphere, *J. Geophys. Res.*, *113*, A09206, doi:10.1029/2007JA012945.

Cladis, J. B. (1986), Parallel acceleration and transport of ions from polar ionosphere to plasma sheet, *Geophys. Res. Lett.*, *13*, 893–896.

Cladis, J. B. (1988), Transport of ionospheric ions in the magnetosphere—Theory and observations, *Adv. Space Res.*, *8*, 165–173, doi:10.1016/0273-1177(88)90283-9.

Cladis, J. B., and W. E. Francis (1992), Distribution in magnetotail of O^+ ions from cusp/cleft ionosphere: A possible substorm trigger, *J. Geophys. Res.*, *97*, 123–130, doi:10.1029/91JA02376.

Cole, K. D. (1965), Stable auroral red arcs, sinks for energy of *Dst* main phase, *J. Geophys. Res.*, *70*, 1689–1706, doi:10.1029/JZ070i007p01689.

Comfort, R. H., I. T. Newberry, and C. R. Chappell (1988), Preliminary statistical survey of plasmaspheric ion properties from observations by DE 1/RIMS, in *Modeling Magnetospheric Plasma, Geophys. Monogr. Ser.*, vol. 44, edited by T. E. Moore and J. H. Waite Jr., pp. 107–114, AGU, Washington, D. C.

Cornwall, J. M., F. V. Coroniti, and R. M. Thorne (1971), Unified theory of SAR arc formation at the plasmapause, *J. Geophys. Res.*, *76*, 4428–4445, doi:10.1029/JA076i019p04428.

Ebihara, Y., M. Yamada, S. Watanabe, and M. Ejiri (2006), Fate of outflowing suprathermal oxygen ions that originate in the polar ionosphere, *J. Geophys. Res.*, *111*, A04219, doi:10.1029/2005JA011403.

Elliott, H. A., R. H. Comfort, P. D. Craven, M. O. Chandler, and T. E. Moore (2001), Solar wind influence on the oxygen content of ion outflow in the high-altitude polar cap during solar minimum conditions, *J. Geophys. Res.*, *106*, 6067–6084, doi:10.1029/2000JA003022.

Fraser, B. J., J. L. Horwitz, J. A. Slavin, Z. C. Dent, and I. R. Mann (2005), Heavy ion mass loading of the geomagnetic field near the plasmapause and ULF wave implications, *Geophys. Res. Lett.*, *32*, L04102, doi:10.1029/2004GL021315.

Funsten, H. O., et al. (2013), Helium, oxygen, proton, and electron (HOPE) mass spectrometer for the radiation belt storm probes mission, *Space Sci. Rev.*, *179*, 423–484, doi:10.1007/s11214-013-9968-7.

Goldstein, J., S. De Pascuale, C. Kletzing, W. Kurth, K. J. Genestreti, R. M. Skoug, B. A. Larsen, L. M. Kistler, C. Mouikis, and H. Spence (2014), Simulation of Van Allen Probes plasmapause encounters, *J. Geophys. Res. Space Physics*, *119*, 7464–7484, doi:10.1002/2014JA020252.

Horwitz, J. L., R. H. Comfort, and C. R. Chappell (1984), Thermal ion composition measurements of the formation of the new outer plasmasphere and double plasmapause during storm recovery phase, *Geophys. Res. Lett.*, *11*, 701–704, doi:10.1029/GL011i008p00701.
Horwitz, J. L., R. H. Comfort, L. H. Brace, and C. R. Chappell (1986), Dual-spacecraft measurements of plasmasphere-ionosphere coupling, *J. Geophys. Res.*, *91*, 11,203–11,216, doi:10.1029/JA091iA10p11203.
Horwitz, J. L., R. H. Comfort, P. G. Richards, M. O. Chandler, C. R. Chappell, P. Anderson, W. B. Hanson, and L. H. Brace (1990), Plasmasphere-ionosphere coupling 2: Ion composition measurements at plasmaspheric and ionospheric altitudes and comparison with modeling results, *J. Geophys. Res.*, *95*, 7949–7959, doi:10.1029/JA095iA06p07949.
Kletzing, C. A., et al. (2013), The electric and magnetic field instrument suite and integrated science (EMFISIS) on RBSP, *Space Sci. Rev.*, *179*, 127–181, doi:10.1007/s11214-013-9993-6.
Kunori, T., M. Nosé, S. Taguchi, K. Hosokawa, M. R. Collier, and T. E. Moore (2007), Storm phase dependence of ion outflow: Statistical signatures obtained by IMAGE/LENA, *Geophys. Res. Lett.*, *34*, L18106, doi:10.1029/2007GL029877.
Lee, J. H., and V. Angelopoulos (2014), On the presence and properties of cold ions near Earth's equatorial magnetosphere, *J. Geophys. Res. Space Physics*, *119*, 1749–1770, doi:10.1002/2013JA019305.
Mauk, B. H., N. J. Fox, S. G. Kanekal, R. L. Kessel, D. G. Sibeck, and A. Ukhorskiy (2013), Science objectives and rationale for the Radiation Belt Storm Probes Mission, *Space Sci. Rev.*, *179*, 3–27, doi:10.1007/s11214-012-9908-y.
Maynard, N. C., and A. J. Chen (1975), Isolated cold plasma regions—Observations and their relation to possible production mechanisms, *J. Geophys. Res.*, *80*, 1009–1013, doi:10.1029/JA080i007p01009.
Moldwin, M. B., L. Downward, H. K. Rassoul, R. Amin, and R. R. Anderson (2002), A new model of the location of the plasmapause: CRRES results, *J. Geophys. Res.*, *107*(A11), 1339, doi:10.1029/2001JA009211.
Moore, T. E., W. K. Peterson, C. T. Russell, M. O. Chandler, M. R. Collier, H. L. Collin, P. D. Craven, R. Fitzenreiter, B. L. Giles, and C. J. Pollock (1999), Ionospheric mass ejection in response to a CME, *Geophys. Res. Lett.*, *26*(15), 2339–2342.
Moore, T. E., et al. (2001), Low energy neutral atoms in the magnetosphere, *Geophys. Res. Lett.*, *28*, 1143–1146, doi:10.1029/2000GL012500.
Nosé, M., K. Takahashi, R. R. Anderson, and H. J. Singer (2011), Oxygen torus in the deep inner magnetosphere and its contribution to recurrent process of O^+-rich ring current formation, *J. Geophys. Res.*, *116*, A10224, doi:10.1029/2011JA016651.
Nosé, M., et al. (2012), *Wp* index: A new substorm index derived from high-resolution geomagnetic field data at low latitude, *Space Weather*, *10*, S08002, doi:10.1029/2012SW000785.
Roberts, W. T., Jr., J. L. Horwitz, R. H. Comfort, C. R. Chappell, J. H. Waite Jr., and J. L. Green (1987), Heavy ion density enhancements in the outer plasmasphere, *J. Geophys. Res.*, *92*, 13,499–13,512, doi:10.1029/JA092iA12p13499.
Singer, H. J., D. J. Southwood, R. J. Walker, and M. G. Kivelson (1981), Alfvén wave resonances in a realistic magnetospheric magnetic field geometry, *J. Geophys. Res.*, *86*, 4589–4596, doi:10.1029/JA086iA06p04589.
Stern, D. P. (1975), The motion of a proton in the equatorial magnetosphere, *J. Geophys. Res.*, *80*, 595–599, doi:10.1029/JA080i004p00595.
Takahashi, K., R. E. Denton, R. R. Anderson, and W. J. Hughes (2006), Mass density inferred from toroidal wave frequencies and its comparison to electron density, *J. Geophys. Res.*, *111*, A01201, doi:10.1029/2005JA011286.
Takahashi, K., S. Ohtani, R. E. Denton, W. J. Hughes, and R. R. Anderson (2008), Ion composition in the plasma trough and plasma plume derived from a Combined Release and Radiation Effects Satellite magnetoseismic study, *J. Geophys. Res.*, *113*, A12203, doi:10.1029/2008JA013248.
Takahashi, K., R. E. Denton, and H. J. Singer (2010), Solar cycle variation of geosynchronous plasma mass density derived from the frequency of standing Alfvén waves, *J. Geophys. Res.*, *115*, A07207, doi:10.1029/2009JA015243.
Takahashi, K., R. E. Denton, M. Hirahara, K. Min, S. Ohtani, and E. Sanchez (2014), Solar cycle variation of plasma mass density in the outer magnetosphere: Magnetoseismic analysis of toroidal standing Alfvén waves detected by Geotail, *J. Geophys. Res. Space Physics*, *119*, 8338–8356, doi:10.1002/2014JA020274.
Tsyganenko, N. A. (1989), A magnetospheric magnetic field model with a warped tail current sheet, *Planet. Space Sci.*, *37*, 5–20, doi:10.1016/0032-0633(89)90066-4.
Tu, J., P. Song, B. W. Reinisch, and J. L. Green (2007), Smooth electron density transition from plasmasphere to the subauroral region, *J. Geophys. Res.*, *112*, A05227, doi:10.1029/2007JA012298.
Volland, H. (1973), A semiempirical model of large-scale magnetospheric electric fields, *J. Geophys. Res.*, *78*, 171–180, doi:10.1029/JA078i001p00171.
Wygant, J. R., et al. (2013), The electric field and waves instruments on the radiation belt storm probes mission, *Space Sci. Rev.*, *179*, 183–220, doi:10.1007/s11214-013-0013-7.

Erratum

In the originally published version of this article, Figures 5, 7, and 9 were reproduced incorrectly in the pdf. This error has been corrected, and this version may be considered the authoritative version of record.